The large format x-ray imager

J. A. Oertel,[a] T. N. Archuleta, and L. S. Schrank
Los Alamos National Laboratory, Los Alamos, New Mexico 87545

(Presented on 20 June 2000)

We introduce a new Large Format X-ray Imaging Camera (LFC) for the Los Alamos National Laboratory (LANL) Inertial Confinement Fusion/Radiation Physics (ICF/RP) program. This instrument is intended as a prototype for use at the National Ignition Facility (NIF), but is capable of operating at LANL's Trident and the University of Rochester's OMEGA laser systems. The LFC is based upon similar x-ray camera architecture and is currently in the final design stages. It is constructed around a mosaic of 3 large (35×105 mm^2) microchannel plate (MCP) detectors, primarily to give a larger field of view, but also for greater temporal coverage and higher magnification while maintaining spatial resolution. The camera is designed to have 30 data channels, six 13-mm-wide microstrips, continuous temporal coverage of 4.2 ns, adjustable electrical gate width, and variable gain on each microstrip and magnifications up to $20\times$. In the process of designing the LFC we scrutinized every element of the gated x-ray imaging process and designed optimization experiments for many of these elements. From the results of two of these experiments, improvements were made in impedance matching to MCPs and, in another, optimization of phosphor on faceplates. [DOI: 10.1063/1.1326005]

I. INTRODUCTION

Gated x-ray imaging cameras have been a primary time-resolved x-ray diagnostic for the National Inertial Confinement Fusion/Radiation Physics (ICF/RP) program for many years.[1] Typically, these instruments use small pinhole arrays to focus x rays onto an image plane with the maximum usable image size limited by the width of the microchannel plate (MCP) microstrip. Most of the instruments currently in use have microstrips or image fields of 6 mm with a few up to 15 mm wide.[2,3] A 6 mm strip with $12\times$ magnification only allows a 0.5 mm object to be imaged. This configuration completely fills the strip and does not allow for any instrument misalignments. What most experimenters regularly do to compensate for the small image field is to focus onto that field with a lower magnification pinhole configuration. This technique works fine up to the point where one requires higher spatial resolution or would simply like to image larger objects while maintaining resolution.

Additionally, most gated instruments are constructed around standard 40 mm MCPs with four microstrips that can be gated independently. When gated, this type of instrument gives researchers a continuous data record up to 1 ns long. This is bounded by the physical length of the microstrip and the propagation velocity of the electrical gating pulse. Researchers have worked around this instrumentation limitation by delaying the time between the individual microstrips and accepting lost temporal information between the strip times. For some experiments with a slower hydrodynamic evolution, this technique is adequate and the missing data contains no useful information. But, for fast moving, long duration (>1 ns) plasma events, longer continuous record lengths can be critical.[4] Because of the design limitations in present instrumentation and the need for a prototype for National Ignition Facility (NIF) instruments, we were motivated to design the Large Format Camera (LFC). See Fig. 1.

The LFC design requirements are (1) to have a wide 13 mm microstrip on the MCP to provide a large field of view with the same or improved spatial resolution, (2) to have six 105 mm microstrips enabling 4.2 ns continuous temporal record, (3) to insert into any standard ICF facility TIM or DIM,[5] and (4) to provide a prototype for the future time-resolved x-ray imager for the NIF.

II. DETAILED INSTRUMENT DESCRIPTION AND SPECIFICATIONS

As with conventional x-ray framing cameras, LFC imaging can be accomplished many different ways. The simplest and least expensive is pinhole imaging.[6] Pinhole imaging uses small pinholes (~5 μm diameter) made of high-Z materials such as tantalum or tungsten. Other methods of imaging include Fresnel zone plate, grazing incident mirror, and crystal imaging.[7–9]

Gating the image is accomplished by launching a short-duration, high-voltage electrical pulse across a microstrip transmission line on a MCP. A photoelectron signal pro-

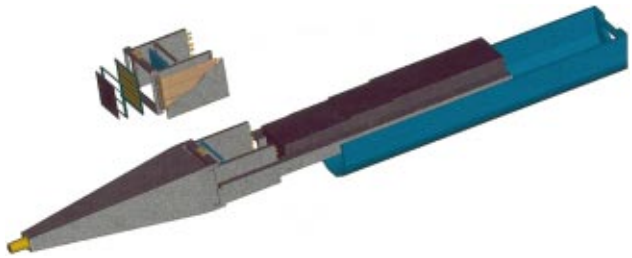

FIG. 1. (Color) The Large Format Camera.

[a]Electronic mail: oertel@lanl.gov

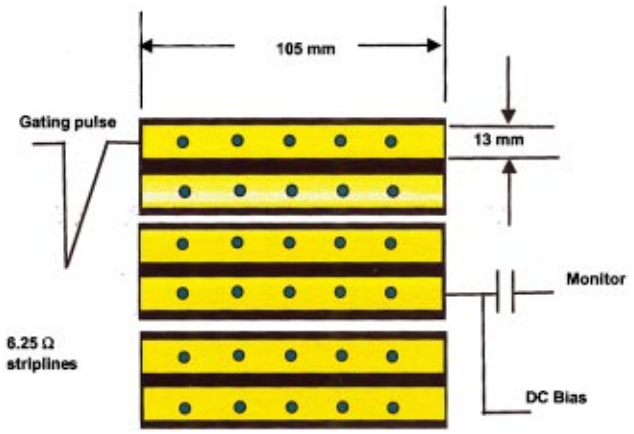

FIG. 2. (Color) Front view of the gated x-ray imaging process with large format MCPs.

duced at the front surface of the MCPs photocathode is then only amplified during the transit time of the voltage pulse across a given point on the microstrip. See Figs. 2 and 3.

The above described process has produced gate times as fast as 40 ps in a MCP with pore length/diameter=40. Amplification or gain of the signal in the MCP scales with the applied pulsed voltage to a large power (20).[2] The impedance, Z, of the microstrip on the MCP decreases with increasing width by the following equation:

$$\frac{w}{h}=\frac{2}{\pi}[(d-1)-\ln(2d-1)]+\frac{\varepsilon-1}{\pi\varepsilon}\times\left[\ln(d-1)+0.293-\frac{0.517}{\varepsilon}\right],$$

where

$$d=\frac{59.95\pi^2}{Z\sqrt{\varepsilon}}$$

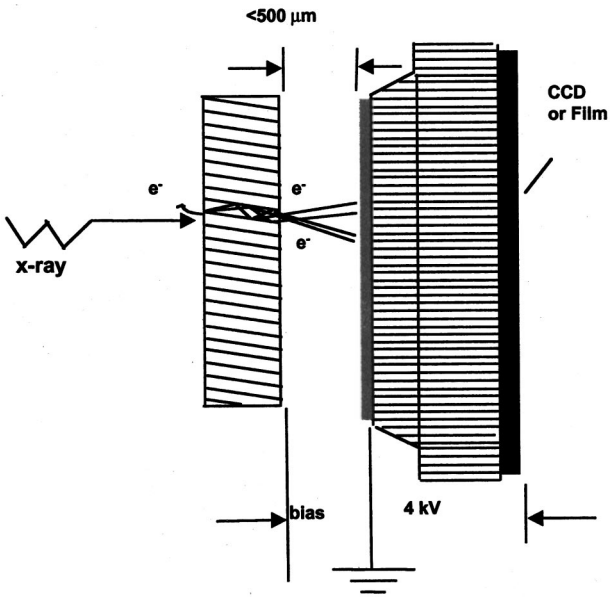

FIG. 3. Side view of the gated x-ray imaging process.

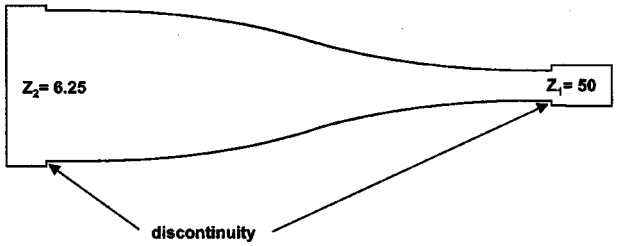

FIG. 4. The Klopfenstein transmission line with discontinuities at each end.

and where w is the width of the strip, h is the dielectric thickness, and ε is the effective dielectric constant.[10] The six 13-mm (6.25 Ω)-wide, 105-mm-long microstrips require a custom impedance matching taper to drive the microstrip from a 50 Ω characteristic impedance. We found that for a given taper length the Klopfenstein impedance taper is optimum in that the reflection coefficient is minimized over the pass-band. The ideal reflection coefficient is obtained by including a discontinuity at each end of the taper as illustrated in Fig. 4. Compared to exponential and Gaussian tapers the Klopfenstein can be 27% shorter, with the same cutoff frequency and band-pass tolerance.[11]

The three large MCPs and six Klopfenstein tapers require a special housing or module in which to be enclosed. This module is designed to capture the three MCPs to an exacting tolerance with respect to each other and the fiberoptic faceplate. In order to accomplish this, a nonconductive high-tensile strength web supports both sides of the three MCPs. This web is then retained in a stainless steel structure that also serves as the ground plane and supports electrical feedthroughs. The 112.5-mm-square fiberoptic faceplate is a composite of thousands of 6 μm fiberoptics compressed together in a coherent array and is coated on one side with P-11 phosphor. As the amplified electrons stream out the back of the MCP array, they collide with the P-11 phosphor emitting visible photons to be collected with film or charged coupled device (CCD) camera.

The electronics designed to run this module are also very specialized. The module requires positive and negative dc voltages to operate MCP and phosphor biases. Each of the six microstrips will be biased independently which require independent control. A six-channel trigger delay circuit enables timing control of each microstrip. Additionally, there are six high-voltage pulsers with selectable pulse widths to drive the MCPs. To determine the pulser voltage to drive a 6.25 Ω strip, we use a combination of past experience and computation.[12] Since power is conserved for the voltage pulse we can state the following:

$$P_{\text{in}}\varepsilon=P_{\text{out}},$$

$$V_{\text{out}}=\sqrt{\frac{R_{\text{out}}\varepsilon(V_{\text{in}})^2}{R_{\text{in}}}},$$

where P is power, ε is the measured taper efficiency, V is voltage, and R is the impedance. We have tested a trial MCP module with a short stripline and an available 2.75 kV, 150 ps pulser for propagation loss and fidelity. The results were in agreement with calculation and are discussed in more de-

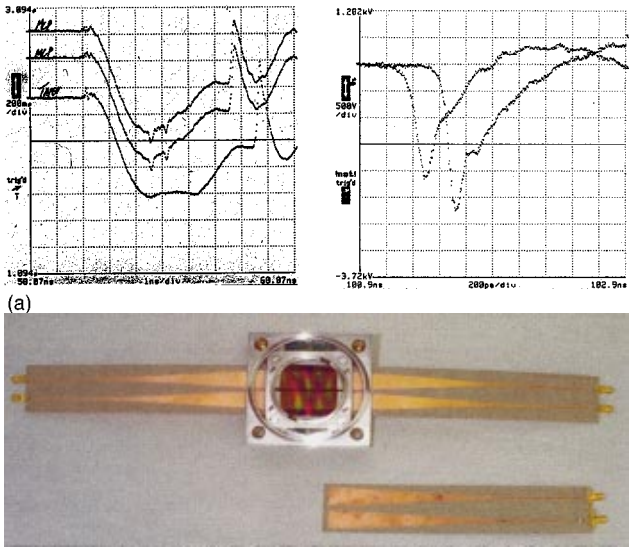

FIG. 5. (a) The left frame shows a time domain reflectometry waveform containing two parallel taper–MCP systems (labeled top strip and bottom strip) and a simple taper for comparison. The impedance starts at 50 Ω and makes a smooth transition to 6.25 Ω with minimal reflections. The right frame shows a waveform of a gating pulse before and after propagation through the taper–MCP system. The system maintains high frequency fidelity and because of minimal reflections has high transmission efficiency. (b) (Color) Prototype module with Klopfenstein taper–MCP system.

tail in Sec. III A. We are in the process of procuring the more complex, higher voltage commercial pulsers which also have all electrical functions controlled by remote computer.[13]

III. INSTRUMENT DESIGN EXPERIMENTS

In designing the LFC we scrutinized every element of gated x-ray imaging and designed optimization experiments for many of these elements. We will briefly describe two of the studies completed.

A. Experimental verification of the Klopfenstein taper

In order to verify calculated performance of the Klopfenstein tapered transmission line, a prototype taper was matched to a MCP with a 13-mm microstrip. The taper has a 50 Ω SMA edge connector installed on one end and was butt-contacted with a compression pad on the MCP side. First, a time domain reflectometry (TDR) trace was taken to observe the impedance transition as a function of length along the taper. As seen in the overlay in Fig. 5, the taper makes a smooth transition between 50 and 6.25 Ω with minimal reflections. Second, a measurement was made using a microwave spectrum analyzer to verify that the reflected power was less than 5% of the input power over the design pass-band (600 MHz to 10 GHz). Finally, we injected a short, high-voltage pulse (2.75 kV, 150 ps) through the system. Observing the pulse before and after the taper–MCP system, it can be seen in Fig. 5 that the taper acts as a high-pass filter, maintains high frequency fidelity, and transmits the pulse with 89% efficiency. This high efficiency allows a lower voltage pulse to be generated in 50 Ω, resulting in an overall cost savings.

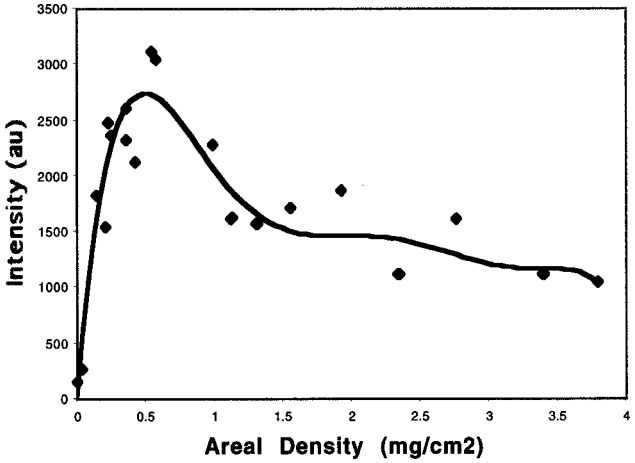

FIG. 6. Phosphor areal density versus intensity.

B. Phosphor coating studies

Most x-ray imaging cameras using film as the recording media use P-11 phosphor. P-11 has a peak wavelength output centered around 460 nm and has a high photographic film exposure efficiency. The coating of phosphor onto the fiberoptic faceplate is performed at LANL by the Diagnostic Engineering Team. The phosphor is purchased presifted to <5 μm particle size and is filtered a second time at LANL for any packing during shipment. The phosphor is mixed with lacquer thinner in a slurry and sprayed on a slowly rotating faceplate for uniformity.

We were interested in knowing how much phosphor was needed to give the maximum output signal and the best possible spatial resolution. To determine this we started with a group of identical fiberoptics and coated each with a slightly different phosphor areal density (0–4 mg/cm^2). We then put each of these screens onto a MCP module that was attached to a dc x-ray source. The MCP module also had a CCD camera attached to it to record output intensity. With the same x-ray source, MCP, and CCD parameters, we systematically observed each screen with various phosphor coatings. The results (Fig. 6) show that, as expected, the 0 mg/cm^2 coating yields 0 output flux. As the coating areal density increased to 0.6 mg/cm^2 the output flux reached a maximum output, which also represented a near 100% phosphor area coverage. From 0.6 to 4 mg/cm^2 the output flux slowly decreased. This is attributed to the multiple layers of phosphor material attenuating the light created at the initial phosphor surface.

To measure the effect of phosphor areal density on relative spatial resolution we placed a resolution test pattern made of a high-Z material (gold) directly on the front face of the MCP and then exposed the MCP to x rays with the same setup as described above. After acquiring the data set, a lineout was taken across a well-defined edge and the 10–90 width was determined for each phosphor areal density. The results (Fig. 7) show that as the areal density of phosphor decreases the spatial resolution increases slightly. The 10–90 width as a function of areal density is roughly related by

$$Y = 3X + 74,$$

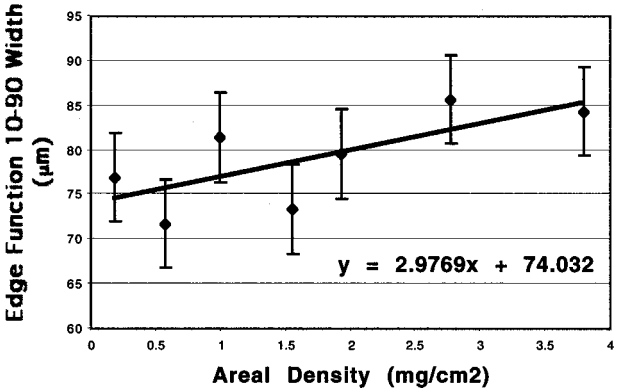

FIG. 7. Phosphor areal density versus spatial resolution.

where Y is the width measured at the 10–90 points and X is the areal density. These results are somewhat incomplete since we know that there will be no spatial resolution when the areal density goes to zero. Thus, the above equation is only reasonable for densities from 0.25 to 3.5 mg/cm^2 of phosphor.

Based on the results of intensity and resolution as a function of phosphor areal density we routinely deposit 0.6 mg/cm^2 of P-11 phosphor on all our fiberoptic faceplates.

IV. CONCLUSIONS

The LFC is a new LANL x-ray imaging instrument designed to image large objects with a long continuous temporal history while maintaining spatial resolution. This camera is also being used to evaluate new technologies that will be applied to future NIF x-ray imagers.

ACKNOWLEDGMENTS

The authors wish to thank the LANL P-24 Technical Staff and the Diagnostic Engineering and Operations Team, especially Scott Evans and Peter Walsh. This work was performed under the auspices of the U.S. Department of Energy by Los Alamos National Laboratory under Contract No. W-7405-Eng-36.

[1] J. D. Kilkenny, Laser Part. Beams **9**, 49 (1991).
[2] O. L. Landen, P. M. Bell, J. A. Oertel, J. J. Satariano, and D. K. Bradley, *Ultrahigh- and High-Speed Photography, Photonics, and Videography '93*, SPIE Vol. 2002 (SPIE, Bellingham WA, 1993), p. 2.
[3] S. Evans *et al.*, Rev. Sci. Instrum. (to be published).
[4] C. W. Barnes *et al.*, Rev. Sci. Instrum. **70**, 471 (1999).
[5] Ten Inch Manipulator (TIM) and Diagnostic Instrument Manipulator (DIM) are mechanisms to insert instruments into spherical ICF target chambers.
[6] A. J. Toepfer, L. P. Mix, and H. J. Trussell, Proc. SPIE **106**, 47 (1977).
[7] A. V. Baez, J. Opt. Soc. Am. **51**, 405 (1961).
[8] F. J. Marshall, M. M. Allan, J. P. Knauer, J. A. Oertel, and T. Archuleta, Phys. Plasmas **5**, 1118 (1998).
[9] F. J. Marshall and J. A. Oertel, Rev. Sci. Instrum. **68**, 735 (1997).
[10] L. A. Trinogga, G. Kaizhou, and I. C. Hunter, *Practical Microstrip Design*, 1st ed. (Horwood, Chichester, England, 1991), p. 30.
[11] R. W. Klopfenstein, Proc. IRE **44**, 31 (1956).
[12] J. A. Oertel, T. Archuleta, F. J. Marshall, and C. G. Peterson, Rev. Sci. Instrum. **68**, 789 (1997).
[13] Grant Applied Physics, Inc., San Francisco, CA.